Ganymede's Ionosphere observed by a Dual-Frequency Radio Occultation with Juno

Ganymede's Ionosphere observed by a Dual-Frequency Radio Occultation with Juno

D. R. Buccino[1] , M. Parisi[1], E. Gramigna[2], L. Gomez-Casajus[3], P. Tortora[2,3], M. Zannoni[2,3], A. Caruso[2], R.S. Park[1], P. Withers[4], P. Steffes[5], A. Hodges[5], S. Levin[1], S. Bolton[6]

[1] Jet Propulsion Laboratory, California Institute of Technology

[2] Department of Industrial Engineering, Alma Mater Studiorum - Università di Bologna, Italy

[3] Centro Interdipartimentale di Ricerca Industriale Aerospaziale, Alma Mater Studiorum - Università di Bologna, Italy

[4] Boston University, Boston, MA

[5] School of Electrical and Computer Engineering, Georgia Institute of Technology

[6] Southwest Research Institute, San Antonio, Texas

Corresponding author: Dustin R. Buccino (Dustin.R.Buccino@jpl.nasa.gov)

Key Points:

- A dual-frequency radio occultation experiment of Ganymede's ionosphere was conducted with the Juno spacecraft on June 7, 2021
- Ingress observed an ionosphere with peak density 2000 +/- 500 (1-σ) cm^{-3} but no statistically significant signature was detected on egress
- Ingress detection occurred in the open field line region, where higher electron impact ionization rates may increase the electron density

Abstract

In June 2021, the Juno spacecraft executed a close flyby of Ganymede. During the encounter, Juno passed behind Ganymede for 15 minutes as observed from Earth, providing the geometry to conduct a radio occultation experiment to probe Ganymede's tenuous ionosphere. X-band and Ka-band radio links were transmitted from Juno to antennas at the Deep Space Network. Electrons encountered along the radio propagation path advance the signal's phase and a linear combination the two frequencies allows for a direct measurement of the electron content along the propagation path. On occultation ingress, an ionosphere peak of 2000 +/- 500 (1-σ) cm^{-3} near the surface was observed. On occultation egress, no statistically significant ionosphere was detected. Ingress observation viewed where Ganymede's intrinsic magnetic field lines are open whereas egress observation viewed where the field lines are closed, implying electron impact ionization plays a key role in the generation of the ionosphere.

Plain Language Summary

Juno conducted a flyby of Ganymede, the largest Galilean moon of Jupiter, on June 7, 2021. During the flyby, the Juno spacecraft set behind Ganymede as observed by the Earth. Juno's radio signals were captured by the Deep Space Network during this time to make radio occultation measurements of Ganymede's ionosphere. Elevated electron density was measured on occultation ingress but no statistically significant ionosphere was detected on egress. These results are consistent with Galileo's radio occultation observations and provide insight into the generation mechanisms of Ganymede's ionosphere.

1 Introduction

The Galilean moons of Jupiter are known to have atmospheres and ionospheres, detected with both ground-based observations and spacecraft data. An oxygen-hydrogen atmosphere was discovered on Ganymede with observations by the Hubble Space Telescope (Hall et al., 1998). Ganymede is a unique object in the solar system in that it has its own intrinsic magnetic field which interacts with the Jovian magnetosphere (Kivelson et al, 1997). Within the open field line regions at higher latitudes, sputtering generates an atmosphere of molecular oxygen subject to ionization and dissociated excitation from the Jovian magnetosphere (Eviatar et al., 2001). Within closed field line regions, it is expected the atmosphere is produced by sublimation (Alexander et al., 1999). It is thought the ionosphere is generated from the neutral atmosphere via photoionization and electron impact from the Jovian magnetosphere (Carnielli et al., 2019). Prior to Juno's encounter with Ganymede, the only direct measurements of Ganymede's ionosphere were those acquired in-situ measurements from the Galileo particle detectors and by the Galileo radio occultation experiment. Due to the flyby distance of the in-situ spacecraft measurements, radio occultation data provide valuable information about the electron densities near the surface of Ganymede.

The Galileo spacecraft executed a total of eight S-band radio occultations of Ganymede throughout its mission, resulting in five non-detections, two weak detections, and one strong detection of an ionosphere (McGrath et al., 2004). To the best of our knowledge, the Galileo radio science data at Ganymede were never archived. In particular with respect to Ganymede, only occultation profiles from the G8 encounter were ever published in scientific literature. The strong ionosphere detection occurred during the Ganymede G8 egress occultation resulting in a peak

electron density of ~5000 cm^{-3} near the surface (Kliore, 1998). Initially, the lack of detection was surprising, but it was hypothesized that positive detections occurred where the trailing hemisphere (where the magnetospheric plasma impacts the moon) of the satellite was in sunlight; therefore, the atmosphere created by sputtering effects from the Jovian magnetosphere can be can be ionized by solar radiation to produce an observable ionosphere (Kliore et al., 2001).

On June 7, 2021, the Juno spacecraft performed a close flyby of Ganymede (Hansen et al., 2022). During this flyby, the spacecraft was occulted by Ganymede as viewed from Earth. Coherent radio links were established during the flyby to enable a radio occultation experiment and gravity experiment to investigate the interior structure (Gomez-Casajus et al., 2022). This article presents the analysis and results of Juno's radio occultation experiment at Ganymede. It is concluded with an interpretation of the resultant ionospheric electron density profiles in the context of current knowledge of Ganymede's tenuous atmosphere and variable ionosphere.

2 Occultation Experiment with Juno

The Juno Gravity Science Instrument (Asmar et al., 2017) is a radio science instrument which utilizes dual-frequency X-band (8.4 GHz) and Ka-band (32 GHz) radio links between the Juno spacecraft and the Earth-based observing stations of NASA's Deep Space Network (DSN). On June 7, 2021 Juno's extended mission trajectory took the spacecraft on a close encounter with Ganymede at an altitude of 1045 km. An Earth occultation occurred during this flyby as shown in Figure 1. Geometric information is summarized in Table 1. Measurement of Ganymede's ionosphere is made via a radio occultation geometry, where the Juno spacecraft set behind Ganymede as observed from Earth. In this way, the radio ray path propagates directly through the ionosphere of Ganymede twice, once on ingress and once on egress. During the radio occultation, Juno transmitted dual-frequency X-band and Ka-band to the 70-meter DSS-43 and 34-meter DSS-35 antennas at the Canberra DSN complex. The occultation experiment was executed in a coherent mode with the downlink signal coherent with the uplink. Both downlink signals were referenced to a single X-band uplink signal sent from the DSS-35 antenna.

Several hours prior to occultation, the DSS-35 antenna transmitted an X-band uplink signal to the spacecraft with a typical uplink acquisition sweep. The acquisition sweep transmits a range of frequencies (+/- 10 kHz at 200 Hz/sec) around the spacecraft transponder's best lock frequency which takes 170 seconds to execute. The transponder locked to this signal and phase-coherently transmitted X-band and Ka-band back to Earth at ratios of 880/749 and 3360/749, respectively. Upon occultation ingress, the transponder unlocked from the uplink signal due to the loss of signal. In order to re-acquire the signal as quickly as possible on egress, a "snap-lock" technique was utilized. In a snap-lock, an uplink acquisition sweep is not executed and instead relies on precisely targeting the spacecraft transponder's best lock frequency to within the pull-in range of 1.3 kHz. For this technique, two effects are carefully considered: a prediction of the oscillator frequency based upon the temperature of the oscillator; and a prediction of the estimated Doppler shift in the uplink signal. The snap-lock on egress was successful and the transponder re-locked to the uplink signal less than 1 second after geometric occultation egress (corresponding with ~5.9 km in altitude). Due to the fast flyby velocity (~18.6 km/sec), without a snap-lock, egress occultation data would have been lost.

3 Methodology

Radio occultation experiments are well-known planetary science methods widely used to perform remote sensing of planetary atmospheres of Solar System bodies, in particular to retrieve vertical profiles of ionosphere electron density and neutral atmosphere physical quantities. The basics of radio occultation experiments for planetary science applications have been presented by (Fjeldbo and Eshleman, 1965; Kliore et al., 1965; Fjeldbo and Eshleman, 1968; Phinney and Anderson, 1968; Fjeldbo et al., 1971). In this technique, the spacecraft transmits a radio signal from the onboard radio to Earth, where it is received by a large ground antenna. As the spacecraft sets behind an object, as viewed from Earth, the radio link will propagate through the object's atmosphere and ionosphere, and it experiences refraction. While investigating ionospheres, refraction due to electrons encountered along the radio ray path causes the signal to bend towards regions of higher index of refraction. This bending produces a phase change in the radio signal proportional to the electron content encountered along the ray path, and it is measured by the ground receiver as a frequency shift. In this context, a dual-frequency analysis is particularly powerful, since it isolates the effect of free-electrons and allows to derive the total electron content and, under certain hypotheses, the local electron density. This analysis adapts methodology as described by Phipps and Withers (2017) and Dalba and Withers (2019) which is briefly described in the following sections.

3.1 Signal Processing

Radio Science utilizes radiometric tracking data collected by the DSN. The preferred method for radio occultation experiments utilizes the Open-Loop Receivers (OLR). The OLR digitally down-converts and records the full spectrum at a user-defined sample rate. The OLR relies on predicted downlink frequencies based on the Doppler shift caused by the motion of the spacecraft trajectory to remain tuned to the incoming signal, without having a feedback loop to be used to track and lock the received signal. This is particularly advantageous in radio occultation experiments, where it is challenging to establish and/or maintain the signal lock near the surface where the signal will be lost and re-acquired. Occultation data were processed from open-loop recordings at 1 kilosamples per second (in-phase and quadrature). The frequency time series are retrieved by processing the OLR data through a spectral fast-Fourier transform algorithm (Paik and Asmar, 2011), in order to obtain a sufficiently high number of frequency measurements. Due to the fast flyby of Ganymede by Juno, the integration time-step of 1 second was selected. This resulted in a satisfactory trade-off between the number of measurements in order to have enough vertical resolution to probe Ganymede's tenuous ionosphere, and the thermal noise.

3.2 Differential Frequency Technique

The differential frequency, or dual-frequency, technique uses two frequencies simultaneously to determine the structure of a planetary body's ionosphere. This method allows for the removal of the classical Doppler shift, as well as the non-dispersive effects, such as neutral atmosphere contributions, and the time variation of the uplink frequency as seen by the spacecraft (clock source). In this way it is possible to isolate the effect of free electrons, which is frequency dependent, on rays traversing the ionosphere.

As shown in Equation 1 (Dalba and Withers, 2020), the received frequency, f_R, differs from the transmitted frequency, f_T. This is due to the classical Doppler shift (which can be computed using Equation 1 of Schinder et al. 2015), a shift due to plasma along the ray path, and a shift due to neutral gas along the ray path, respectively. The frequency shift due to the charged particles is

inversely proportional to the transmit frequency f_T. In this way, it is possible to take advantage of multiple frequencies to directly measure the electron content along the radio ray path.

$$f_R = f_T - \frac{f_T}{c}\frac{d}{dt}\int dl + \frac{e^2}{8\pi^2 m_e \varepsilon_0 c f_T}\frac{d}{dt}\int N_e dl - \frac{f_T \kappa}{c}\frac{d}{dt}\int n dl \quad (1)$$

where l is the path length, c is the speed of light, t is time, e is the elementary charge, m_e is the electron mass, ϵ_0 is the permittivity of free space, N_e and n are the electron density and neutral density at a given point, respectively, and κ is the refractive volume of neutral gas at a given point.

During the occultation, the spacecraft transmitted frequencies at X-band ($f_{T,X}$) and at Ka-band ($f_{T,Ka}$). The frequencies precisely related by the ratio of the turnaround ratios, i.e. $f_{T,Ka}/f_{T,X}$ = 3360/880. Differential frequency residuals are then obtained as a function of time in Equation 2.

$$\Delta f(t) = f_{R,X}(t) - \frac{880}{3360} f_{R,Ka}(t) = \frac{e^2}{8\pi^2 m_e \varepsilon_0 c f_{T,X}}\left(1 - \left(\frac{880}{3360}\right)^2\right)\frac{d}{dt}\int N_e dl \quad (2)$$

As a result, the plasma column density along the ray path $\int N_e dl$, or Total Electron Content (TEC), as a function of time, can be directly obtained from time series of received frequencies at X- and Ka-band. Because the dual-frequency link is only present on the downlink, the retrieved TEC is referred to the downlink radio ray path only.

Before obtaining the TEC and local electron density, it is crucial to calibrate the differential frequency residuals of Equation 2 for the solar plasma and Earth's ionosphere, in order to obtain reliable results. If not calibrated, these effects could jeopardize the accuracy of the retrieved electron densities. The noises can be evaluated in the baseline of the residual frequencies, the region where the signal is traveling outside the ionosphere of Ganymede. The baseline should be flat with low-noise and zero-mean residual frequencies. In the case of Juno, the largest effect on the dual-frequency residuals is that of the spin-phase wrapping (Marini, 1971). A bias offset is evaluated in the baseline and subtracted to the entire observation time-span of the differential frequency residuals.

After calibration, Equation 2 is integrated with respect to time and obtain the TEC using Equation 3. This is then translated into a function of the closest approach distance of the radio ray path to the center of mass of Ganymede using the spacecraft and planetary ephemerides, where X is the closest approach distance.

$$TEC(X) = \int N_e dl = \int \frac{8\pi^2 m_e \varepsilon_0 c f_{T,X}}{e^2\left(1 - \left(\frac{880}{3360}\right)^2\right)}\Delta f(t) dt \quad (3)$$

Following (Dalba and Withers, 2020), and assuming that Ganymede's ionosphere is locally spherically symmetric, the vertical profiles of Ganymede's electron density are obtained using an Abel transform inversion formula, starting from the TEC (Fjeldbo et al., 1971; Hinson et al., 1999; Withers, 2020) using Equation 4.

$$N_e(r) = \frac{1}{\pi}\int_{X=r}^{X=\infty} \ln\left(\frac{X}{r} + \sqrt{\left(\frac{X}{r}\right)^2 - 1}\right) d\left(\frac{dTEC(X)}{dX}\right) \quad (4)$$

where r is the radial distance. Consequently, the vertical profile of the ionospheric electron density $N_e(r)$, is derived from the integrated plasma column density (TEC). In the Abel transform, it is assumed that the ionosphere is spherically symmetric at the occultation point. The non-spherical nature of Ganymede's ionosphere could possibly lead to biases in electron density results at the icy moons of Jupiter in certain geometries (Kliore 1998). However, since the index of refraction of the ionosphere is very small (it deviates from 1 by about 10^{-9} in the part of the ionosphere where the electron density is maximum), the rays do not bend significantly and they can safely be assumed to follow straight lines. Thus, the Abel transform should still result in accurate electron density profiles, for example, as assumed for Saturn and Titan (Schinder 2020).

4 Results

The analysis of the ingress leg of the experiment uses data beginning at 16:48:00.0 after spacecraft telemetry was turned off, until 17:18:55.1. Although actual loss of signal at Ka-band occurs 1 second later at 17:18:56.1, effects of diffraction are observed and the data cutoff was chosen to occur prior to this (see Text S1 of Supporting Information). The egress leg consists of data between the time of signal re-acquisition at 17:32:38.0 until the 17:52:00.0 when a second re-acquisition sweep was executed. All times are stated in UTC as received on Earth (Earth Receive Time). Because it took the spacecraft transponder ~1-2 seconds to re-acquire the uplink signal on egress, and the non-coherent portion was not used, diffraction does not affect egress.

The ingress occultation occurred in the southern hemisphere of the moon at latitude 59°S, while the egress occultation occurred 15 minutes later in the northern hemisphere at latitude 20°N. In terms of magnetospheric geometry, both ingress and egress occurred near the terminator. The egress occultation point was partially sun-lit as well as contained in Ganymede's magnetospheric wake. As a result, ingress was characterized by a small Ram angle, and egress by a small Solar Zenith angle, and either one (if not both) of these conditions are considered favorable for the detection of an ionosphere.

Figure 2 shows the dual-frequency residuals (in Hz), which were obtained using Equation 2 for ingress (panel a) and egress (panel b). The data were calibrated as described in the previous section, using a baseline defined by ray-path altitudes over Ganymede's surface between 5,000-11,000 km for ingress, and 5,000-7,000 km for egress. These altitude intervals were selected so that the baselines are completely outside of Ganymede's ionosphere. Nevertheless, the results are stable regardless of the baseline chosen to perform the calibrations, down to an altitude of about 1,500 km.

After calibration, the profiles of dual-frequency residuals are directly converted using Equation 3 into profiles of Total Electron Content (TEC), a measure of column density of electrons (10^{16} m^{-2}). The TEC shows there is a clear accumulated ionosphere signal at low altitudes below 800 km during the ingress occultation but such signal is not detected on the egress occultation, which remains relatively constant (see Figure S4 in Supporting Information).

The TEC represents the column density obtained integrating the electron density N_e along the ray path, and is, therefore, an average measurement. To retrieve the local electron density (in

220 cm^{-3}) as a function of altitude, an Abel transform is performed on the TEC profile using Equation
221 4. The key assumption for using this algorithm is that of local spherical symmetry of the satellite
222 around the occultation point. The electron density is plotted once again against the altitude above
223 the surface of the satellite (Figure 3). For both ingress and egress the vertical resolution is ~5.9 km
224 (at 1 second integration time) which is largely dependent on the flyby velocity. In order to mitigate
225 the effect of thermal noise, 1000 electron density profiles were generated by beginning the
226 frequency estimation with subsequent open-loop samples (1000 profiles are generated with a
227 sampling rate of 1 kHz). The profiles were then averaged (see Text S2 in Supporting Information).
228 These results show that there is an elevated electron density near the surface above the 3-σ
229 uncertainty level on ingress (Figure 3a). The peak density is approximately (2000 ± 500) cm^{-3} (1-
230 σ) at a 15 km data cutoff altitude. On ingress between 15 km and 1,500 km, the corresponding
231 scale height H assuming an exponential ionosphere ($e^{-z/H}$) is 1050 ± 110 km. Egress yielded an
232 observation of (400 ± 500) cm^{-3} (1-σ). Although the electron density profile on egress was more
233 sensitive to the calibration techniques, the averaged profile is statistically compatible with zero at
234 the 3-σ level with one exception around 1,800 km. Due to the high altitude and sensitivity to the
235 baseline calibration, is likey not associated with the ionosphere and therefore we conclude egress
236 does not show a detection of an ionosphere (Figure 3b).

237 Thermal, instrumental, and propagation noise sources are present in the data. The
238 dominating noise in the observation is thermal. Instrumental noise is negligible, since the oscillator
239 stability and atmospheric effects cancel in the dual-frequency combination, leaving only hardware-
240 related sources with estimated Allan deviation stability on the order of ~10^{-16} to ~10^{-15} at 1000-sec
241 (Asmar et al 2005). Propagation sources of error from plasma are also present and include
242 fluctuations in the Earth's ionosphere and solar plasma. The local time of the ray path through
243 Earth's ionosphere occurred during night, when ionosphere activity is lower than daytime. These
244 variations in Earth's ionosphere during the occultation timeframe were small as measured by
245 GNSS receivers located at the DSN antennas. When calibrated, it did not change the results. Solar
246 plasma noise is the other propagation noise source. The larger drift trend of solar plasma is
247 removed in the background polynomial fit. Solar plasma scintillation at the solar elongation angle
248 of 105° during Ganymede's occultation corresponds with an X-band scintillation noise of 0.75
249 mHz (after conversion from Asmar et al (2005) from Allan deviation of ~2×10^{-14} at 1000-sec),
250 therefore we do not expect this effect to dominate the data noise when compared with the thermal
251 noise levels of nearly twice that. However, undesired solar plasma noise may still be present in the
252 observation. The error bars (represented by shaded regions) were estimated through means of a
253 Monte Carlo analysis by adding gaussian random noise time-series (whose σ is consistent with the
254 observed noise outside Ganymede's ionosphere) to the original differential frequency residuals, in
255 order to obtain the standard deviations of the profiles in terms of electron density. The 1-σ (~500
256 cm^{-3}) and 3-σ uncertainties (~1500 cm^{-3}) derived from the Monte Carlo analysis is consistent with
257 an uncertainty estimated using the method described by Withers, 2020.

258 **5 Discussion**

259 Ganymede's atmosphere is generated by charged particle sputtering and sublimation from
260 the icy surface with detections by Hubble Space Telescope (Hall et al, 1998 & Roth et al, 2021).
261 In the context of the Juno occultation measurements, ingress and egress occultation points appear
262 to be in ice-rich regions (Ligier et al., 2019) where this can occur. Ganymede's ionosphere is
263 generated from the neutral atmosphere through photo-ionization and electron-impact ionization

from Jupiter's magnetosphere (Carnielli et al., 2019). Juno's radio occultation are observed at the closest point to the surface of Ganymede along the ray path between the spacecraft and Earth. In this geometry, ingress was in the shadow whereas egress was in a sun-lit region (Figure 1). When comparing occultation points with open-closed field line boundaries of Ganymede's magnetosphere (either from Duling et al (2022) or Jia and Kivelson, 2021), it is evident that ingress occurred in the open-field line region and egress likely occurred in the closed-field line regions. Since electron-impact ionization rates would be higher in open field-line regions, the Juno occultation sheds light on the generation mechanisms for Ganymede's ionosphere.

The stark contrast in the geometry of the Juno occultation – ingress in the shadow, but open field-line and egress sun-lit, but in closed field-line region – indicates that electron-impact ionization plays an important role in generating Ganymede's ionosphere in the open-field line region. This is corroborated by the strong detection of the ionosphere by Galileo radio occultation. The G8 egress occultation, occurring at a latitude of 47° N and west longitude of 22° (Kliore 1998), was also in the open field-line region defined by Jia and Kivelson, 2021.

Previous modeling efforts of Ganymede's ionosphere have been conducted by Eviatar et al 2001, Carnielli et al 2019, and Carnielli et al 2020. Eviatar et al 2001 modeled the surface density of electrons is about 400 cm^{-3} with a scale height of 600 km. Near the surface, the scale height may be considerably smaller yielding a higher surface density. Although the modeled surface density is well below an upper limit obtained by the Galileo radio occultation measurement, Eviatar et al 2001 also show that the peak electron densities measured by Kliore (1998) do not contradict a model of the ionosphere in the polar cap region due to large uncertainties in atomic and environmental parameters. Juno's ingress occultation observation of 2000 cm^{-3} is lower than the upper limit set by Galileo G8 egress occultation and thus the Juno occultation results not exclude this upper limit from possibilities either. Extending on Carnielli et al 2019, Carnielli et al 2020 proposed that increasing neutral atmosphere densities or increased electron-impact ionization rates can explain discrepancies between observations and models.

Juno successfully executed a radio occultation of Ganymede during a close encounter on June 7, 2021. Both ingress and egress electron profiles were obtained using a dual-frequency technique. On ingress, an ionosphere signature was detected with a peak electron density of 2000 +/- 500 (1-σ) cm^{-3} at 15 km with a scale height of 1050 ± 110 km. On egress, no statistically significant ionosphere was detected. Thus, at first glance the Juno occultation results appears consistent with results of the Galileo occultation campaign where only one strong detection of an ionosphere was observed with a peak of approximately 5000 cm^{-3} at 16 km (Kliore 1998) out of eight occultation profiles. With current knowledge of the interaction between Ganymede's atmosphere, ionosphere, and Jupiter's magnetosphere, we conclude that the reason for the ability to detect an ionosphere with the radio occultation technique is due to higher electron impact ionization rates in open-field line regions, where positive detections of the ionosphere occur.

Acknowledgments

The work of DB, MP, RP, and SL was carried out at the Jet Propulsion Laboratory, California Institute of Technology, under a contract with the National Aeronautics and Space Administration. Government sponsorship acknowledged.

EG, LGC, PT, MZ and AC are grateful to the Italian Space Agency (ASI) for financial support through Agreement No. 2018-25-HH.0 in the context of ESA's JUICE mission, and Agreement

No. 2017-40-H.1-2020, and its extension 2017-40-H.02020-13-HH.0, for ESA's BepiColombo and NASA's Juno radio science experiments. EG is grateful to "Fondazione Cassa dei Risparmi di Forlì" for financial support of his PhD fellowship.

PS and AH were supported by NASA Contract NNM06AA75C from the Marshall Space Flight Center under subcontract 699054X from Southwest Research Institute.

Data Availability Statement

The Juno radio science data used in this research are publicly available through NASA's Planetary Data System at https://atmos.nmsu.edu/PDS/data/jnogrv_1001/ (Buccino, 2016). The occultation results presented here are provided in a corresponding dataset with this publication on Zenodo (Buccino, 2022).

References

Asmar, S. W., Armstrong, J. W. & Tortora, P. (2005). Spacecraft Doppler tracking: Noise budget and accuracy achievable in precision radio science observations. *Radio Science*, *40*(2), RS2001.

Asmar, S. W., Bolton, S. J., Buccino, D. R., Cornish, T. P., Folkner, W. M., Formaro, R., ... & Simone, L. (2017). The Juno gravity science instrument. *Space Science Reviews*, *213*(1), 205-218.

Buccino, D. R. (2016). Juno Jupiter gravity science raw data set V1.0, JUNO-J-RSS-1 JUGR-V1.0, NASA planetary data system (PDS). Retrieved from https://atmos.nmsu.edu/PDS/data/jnogrv_1001/

Dustin Buccino. (2022). Corresponding Dataset for Ganymede's Ionosphere observed by a Dual-Frequency Radio Occultation with Juno [Data set]. https://doi.org/10.5281/zenodo.6206226

Carnielli, G., Galand, M., Leblanc, F., Leclercq, L., Modolo, R., Beth, A., ... & Jia, X. (2019). First 3D test particle model of Ganymede's ionosphere. *Icarus*, *330*, 42-59.

Carnielli, G., Galand, M., Leblanc, F., Modolo, R., Beth, A., & Jia, X. (2020). Constraining Ganymede's neutral and plasma environments through simulations of its ionosphere and Galileo observations. *Icarus*, *343*, 113691.

Dalba, P. A., & Withers, P. (2019). Cassini radio occultation observations of Titan's ionosphere: The complete set of electron density profiles. *Journal of Geophysical Research: Space Physics*, *124*(1), 643-660.

Duling, S., Saur, J., et al (2022). Ganymede MHD Model: Magnetospheric Context for Juno's PJ34 flyby. *Geophysical Research Letters,* xxx(x), xxx-xxx. (this issue)

Eviatar, A., Vasyliūnas, V. M., & Gurnett, D. A. (2001). The ionosphere of Ganymede. *Planetary and Space Science*, *49*(3-4), 327-336.

Fjeldbo, G. & Eshleman V. R., (1965). The bistatic radar-occultation method for the study of planetary atmospheres. *Journal of Geophysical Research,* 70, 3217.

Fjeldbo, G., & Eshleman, V. R. (1968). The atmosphere of Mars analyzed by integral inversion of the Mariner IV occultation data. *Planetary and Space Science*, *16*(8), 1035-1059.

Fjeldbo, G., Kliore, A. J., & Eshleman, V. R. (1971). The neutral atmosphere of Venus as studied with the Mariner V radio occultation experiments. *The Astronomical Journal*, *76*, 123.

Gomez-Casajus, et al (2022). The Gravity Field of Ganymede after the Juno's Extended Mission. *Geophysical Research Letters,* xxx(x), xxx-xxx. (this issue)

Hall, D. T., Feldman, P. D., McGrath, M. A., & Strobel, D. F. (1998). The far-ultraviolet oxygen airglow of Europa and Ganymede. *The Astrophysical Journal*, *499*(1), 475.

Hansen, C.J., Bolton, S., Brennan, M., Lunine, J. Sulaiman, A., Levin, S., Connerney, J. and Clark G.P., Overview of Juno's Flyby of Ganymede. *Geophysical Research Letters,* xxx(x), xxx-xxx. (this issue)

Hinson, D. P., Simpson, R. A., Twicken, J. D., Tyler, G. L., & Flasar, F. M. (1999). Initial results from radio occultation measurements with Mars Global Surveyor. Journal of Geophysical Research, 104, 26,997–27,012

Jia, X., & Kivelson, M. G. (2021). The Magnetosphere of Ganymede. *Magnetospheres in the Solar System*, 557-573.

Kivelson, M. G., Khurana, K. K., Coroniti, F. V., Joy, S., Russell, C. T., Walker, R. J., ... & Polanskey, C. (1997). The magnetic field and magnetosphere of Ganymede. *Geophysical Research Letters*, *24*(17), 2155-2158.

Kliore, A. J. (1998). Satellite atmospheres and magnetospheres. *Highlights of Astronomy*, *11*(2), 1065-1069.

Kliore, A., Cain, D. L., Levy, G. S., Eshleman, V. R., Fjeldbo, G., & Drake, F. D. (1965). Occultation experiment: Results of the first direct measurement of Mars's atmosphere and ionosphere. *Science*, *149*(3689), 1243-1248.

Kliore, A. J., Anabtawi, A., & Nagy, A. F. (2001, December). The ionospheres of Europa, Ganymede, and Callisto. In *AGU Fall Meeting Abstracts* (Vol. 2001, pp. P12B-0506).

Ligier, N., Paranicas, C., Carter, J., Poulet, F., Calvin, W. M., Nordheim, T. A., ... & Ferellec, L. (2019). Surface composition and properties of Ganymede: Updates from ground-based observations with the near-infrared imaging spectrometer SINFONI/VLT/ESO. *Icarus*, *333*, 496-515.

Marini, J. W. (1971). The effect of satellite spin on two-way Doppler range-rate measurements. *IEEE Transactions on Aerospace and Electronic Systems*, (2), 316-320.

McGrath, Melissa A., et al. "Satellite atmospheres." *Jupiter: The Planet, Satellites and Magnetosphere* (2004): 457-483.

Phipps, P. H., & Withers, P. (2017). Radio occultations of the Io plasma torus by Juno are feasible. *Journal of Geophysical Research: Space Physics*, *122*(2), 1731-1750.

Phinney, R. A., & Anderson, D. L. (1968). On the radio occultation method for studying planetary atmospheres. *Journal of Geophysical Research*, *73*(5), 1819-1827.

Roth, L., Ivchenko, N., Gladstone, G. R., Saur, J., Grodent, D., Bonfond, B., ... & Retherford, K. D. (2021). A sublimated water atmosphere on Ganymede detected from Hubble Space Telescope observations. Nature Astronomy, 5(10), 1043-1051.

Schinder, P. J. (2020). Users Guide for the Cassini Radio Science ionospheric electron density profiles data set for both Saturn and Titan. https://atmos.nmsu.edu/data_and_services/atmospheres_data/Cassini/logs/CasRSS_ionospheres_profiles_users_guide.pdf

Withers, P. (2020). Revised predictions of uncertainties in atmospheric properties measured by radio occultation experiments. *Advances in Space Research*, *66*(10), 2466-2475.

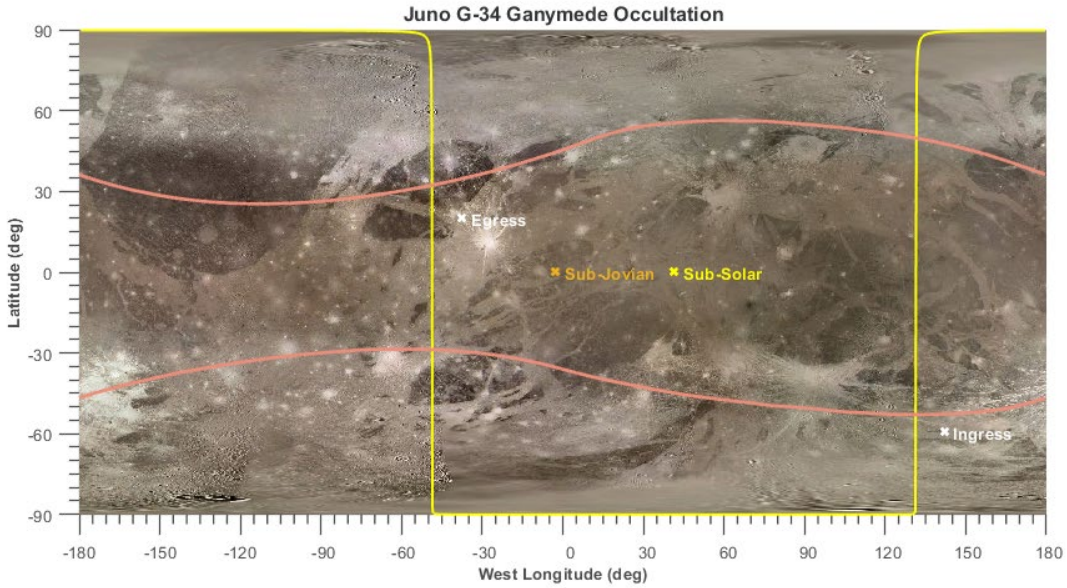

Figure 1. Geometry of the Juno G-34 flyby and radio occultation points. The occultation ingress point was just outside the terminator at -142°W / 59°S and egress occurred just inside the terminator near the spacecraft ground track at 38°W / 20°N. The spacecraft ground track is shown

in white, sun terminator in yellow, and sub-Jovian point in orange. Overlaid in light red are the open/closed field line boundaries from Duling et al (2022).

Table 1. Geometry of the Juno radio occultation of Ganymede. Parameters are given at the occultation point (closest point along the radio propagation path to Ganymede).

Observation	Occultation Time (UTC Earth Receive)	Distance (km)	Lat. (deg)	W. Long. (deg)	Solar Zenith Angle (deg)	Ram Angle (deg)
Juno G34 Ingress	2021-Jun-07 17:18:57	18,094	59° S	-142° W	95°	72°
Juno G34 Egress	2021-Jun-07 17:32:38	3,772	20° N	38° W	80°	125°

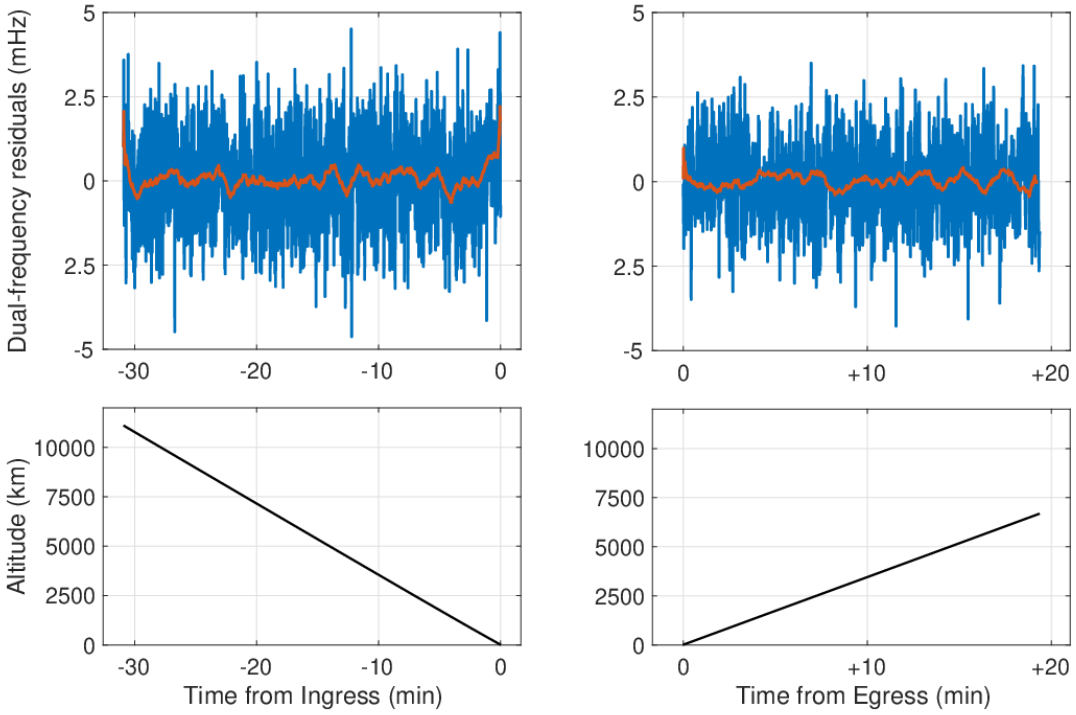

Figure 2. Plots of the 1-second integration time (blue) and 60-second average (red) dual-frequency residuals (Hz) for the ingress (a) and egress (b) occultations as a function of time, along with plots of the ray path altitude over the surface of Ganymede (c, d), during the occultations.

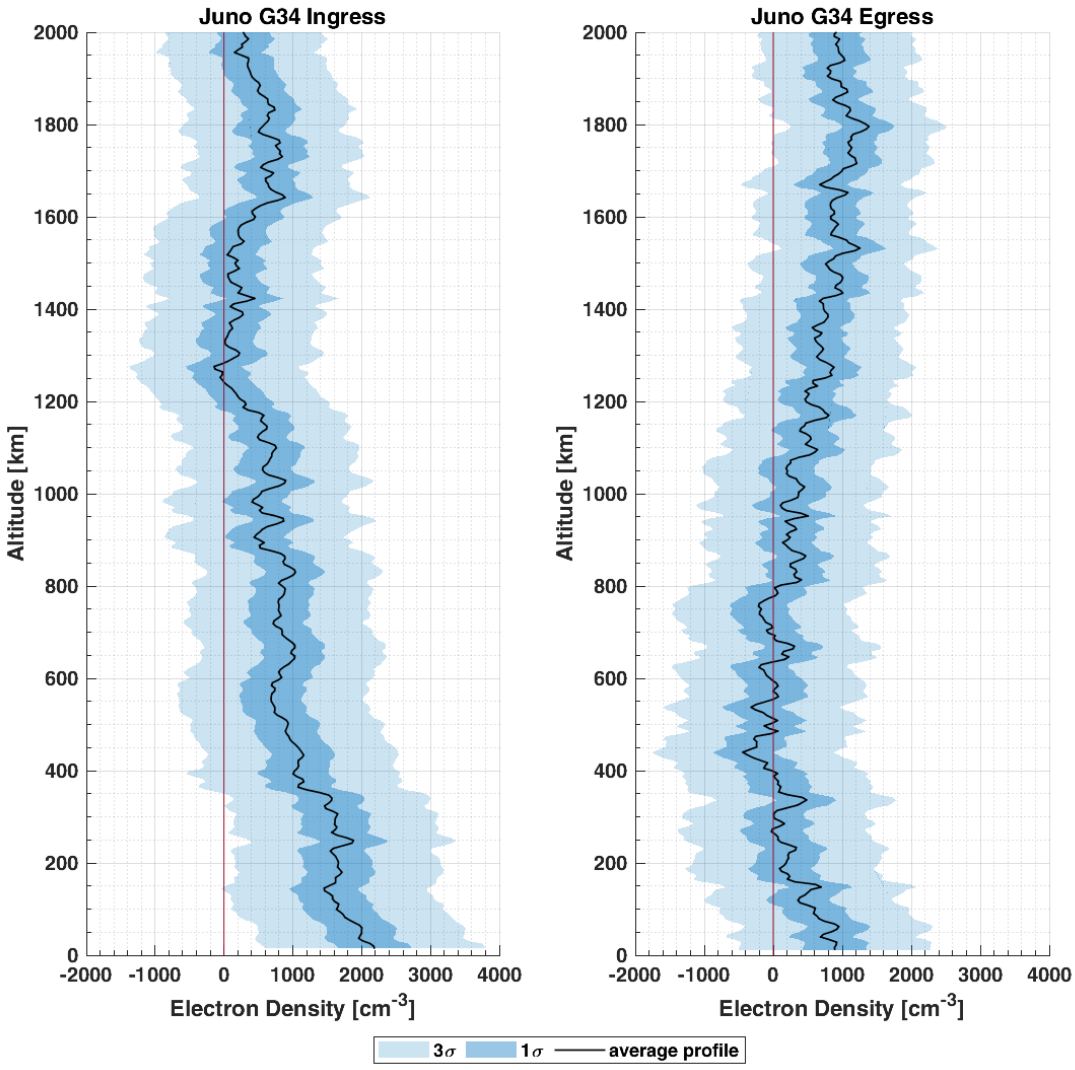

404

405 **Figure 3**. Electron density within Ganymede's ionosphere during ingress occultation (a) and
406 egress occultation (b). The dark and light blue shaded area represent the 1-σ and 3-σ uncertainties,
407 respectively.